On the nature of early-type galaxies

Krajnović, D.

Chapter 4

Kinemetry: a method to quantify kinematic maps

Davor Krajnović, Michele Cappellari, Yannick Copin, P. Tim de Zeeuw, to be submitted to Monthly Notices of the Royal Astronomical Society

We present a general method for analysing and describing kinematic maps of galaxies observed with integral-field spectrographs. It is based on a harmonic expansion of the maps along concentric rings in the plane of the sky, similar to the expansions used to quantify observed HI, CO and Hα velocity fields, and analogous to standard surface-photometry methods for analysing broad-band imaging. We call our method kinemetry. We analyse the kinematic moments (mean velocity, velocity dispersion and higher-order Gauss–Hermite moments of the line-of-sight velocity distribution) of a model elliptical galaxy, and discuss the meaning of the amplitude coefficients and corresponding phases of the expansion. The observed kinematic moments have certain symmetries in the plane of the sky, and we exploit these to filter the maps. We present diagnostics for determining the consistency of velocity maps with axisymmetric underlying geometry, based on the phase angles of the first two odd terms of the expansion. We apply this method to SAURON observations of the galaxy NGC 4365 and quantify the departures from axisymmetry. We consider kinemetric expansions along circular and elliptic annuli, and find that expansion along suitably-chosen ellipses may be superior for maps of the mean velocity and the higher-order odd moments, while circles may be more suited for velocity dispersion maps and the higher-order even moments. We present evidence that the velocity maps of some early-type galaxies closely resemble the observed kinematics of inclined circular disks, but the generality of this result needs to be investigated further.

1 Introduction

TWO-DIMENSIONAL velocity maps were, until recently, largely the privileged property of radio astronomers. The advantages of full two-dimensional spatial coverage of extended astronomical objects are self-evident and are extensively used in e.g. HI studies of disk galaxies. The advent of integral-field spectrographs (IFS) has brought two-dimensional kinematic measurements to optical wavelengths.

The inclusion of optical wavelengths also broadens the variety of objects accessible for study. The two-dimensional radio observations are dependent on the existence of

gas, while optical observations probe both the stellar absorption- and gas emission-line spectral features, which may co-exist in the same potential with very different spatial distributions and dynamical structures. The wealth of features seen in the stellar kinematic maps of early-type galaxies (Emsellem et al. 2004) confirms the usefulness of two-dimensional data, but also poses a problem of efficiently harvesting and interpreting the important features from the maps.

An approach using harmonic expansion was developed for the analysis of the two-dimensional radio velocity maps. This method divides a velocity map into individual rings (the so-called tilted-ring method, Begeman 1987) with a harmonic expansion along these rings (e.g. Binney 1978; Teuben 1991). Assuming that the velocity map is generated by gas moving in a thin disk, it is possible to assign certain physical properties to the coefficients of the harmonic expansion: e.g. the first *cosine* term in the expansion gives the circular velocity of the gas, assuming the gas moves in circular orbits in the disk. The higher-order terms measure the departures from a simple disk model (pure circular motion) caused by e.g. elongation of the potential. This approach was pioneered by Franx et al. (1994) and Schoenmakers et al. (1997) who used it to investigate the axisymmetry of spiral galaxies, based on the prediction for harmonic coefficients coming from epicyclic theory. Recently Wong et al. (2004) used this method as a diagnostic tool for measuring radial flows in spiral galaxies.

The harmonic expansion is a simple and straight-forward tool to extract information from two-dimensional maps, and is a natural method for harvesting information from kinematic maps obtained by the new optical IFS. However, interpretation of the results depends on the intrinsic nature of galaxies. The spheroidal distribution of stars typical of early-type galaxies does not have the same dynamical properties as a gas disk. To explore those intrinsic properties, we need a more general description of the harmonic terms, without assumptions on geometry or dynamical state of the observed system. In this paper we present such a method, which we call *kinemetry* due to its complementarity with surface photometry of early-type galaxies. In its basics, kinemetry is a generalisation of the tilted ring harmonic expansion method for analysing velocity maps of gaseous discs to the kinematic observations of spheroidal systems such as elliptical and lenticular galaxies.

In Section 2 we present the theoretical background on which kinemetry operates. Section 3 presents the method and discusses two choices of expansion: along circles and along ellipses. The meaning of the kinemetric coefficients for different kinematic moments is presented in Section 4. In Section 5 we present the application of kinemetry as a diagnostic tool for quantifying axisymmetry and kinemetric misalignments in triaxial systems, and we discuss the advantages of the expansion along ellipses. Section 6 summarises the conclusions.

2 Theoretical background and motivation

The dynamics of a collisionless stellar system is fully specified by its phase-space density or distribution function $f = f(\vec{x}, \vec{v}, t)$ (e.g. Binney & Tremaine 1987). However, this quantity is not measurable directly. When observing external galaxies, we measure properties that are integrated along the line-of-sight (LOS). The observables, which

reveal only the averages of properties of a large number of unresolved stars, are the surface brightness and the full velocity profile (for a review see de Zeeuw 1994). An additional complication is that the galaxies are viewed from a certain angle, and we actually observe only the projected properties of the integrated distribution function.

Analysis of the projected surface brightness via (broad-band) imaging is called *surface photometry*. The surface brightness is, however, only the zeroth-order projected moment of the distribution function. For a complete picture, the analysis has to include the full velocity profile, i.e. the line-of-sight velocity distribution (LOSVD):

$$\mathcal{L}(v; x, y) = \int_{\mathrm{LOS}} \mathrm{d}z \int\int \mathrm{d}v_x \mathrm{d}v_y \, f(\vec{r}, \vec{v}), \tag{1}$$

where (*x*,*y*,*z*) are the three spatial coordinates, oriented such that the LOS is along the *z*-axis. Observations of the LOSVD are usually presented by its moments: mean velocity V, velocity dispersion σ and higher-order moments commonly parametrised by Gauss-Hermite coefficients, (van der Marel & Franx 1993; Gerhard 1993), h_3 and h_4 being the most commonly used.

The kinematic moments of stationary triaxial systems show a high degree of symmetry which can be expressed through their parity. The mean velocity is an odd moment, while velocity dispersion is an even moment. In practice, this means that a two-dimensional map of a given moment shows corresponding symmetry. Maps of even moments are *point-symmetric*, while maps of odd moments are *point-anti-symmetric*. In polar coordinates this gives:

$$\begin{aligned} \mu_e(r, \theta + \pi) &= \mu_e(r, \theta), \\ \mu_o(r, \theta + \pi) &= -\mu_o(r, \theta), \end{aligned} \tag{2}$$

where μ_e and μ_o are arbitrary even and odd moments of the LOSVD, respectively. Furthermore, if the observed system is axisymmetric, the even moment of the LOSVD will also be *mirror-symmetric* or, correspondingly, an odd moment will be *mirror-anti-symmetric*:

$$\begin{aligned} \mu_e(r, \pi - \theta) &= \mu_e(r, \theta), \\ \mu_o(r, \pi - \theta) &= -\mu_o(r, \theta). \end{aligned} \tag{3}$$

Unlike surface brightness images, analysis of maps of stellar kinematic moments for early-type galaxies have not been extensively explored, due to the small number of studies with full two-dimensional kinematics. On the theoretical front, there were some studies of velocity maps of triaxial systems (e.g. Franx et al. 1991; Statler 1991, 1994a; Statler & Fry 1994; Statler 1994b; Arnold et al. 1994). The new observations with the IFS SAURON (Bacon et al. 2001), and its survey of a representative sample of nearby galaxies (de Zeeuw et al. 2002) yield high-quality maps of the kinematic moments of early-type galaxies (Emsellem et al. 2004). The structures visible on these kinematic maps are reflections of the intrinsic properties of the galaxies and kinemetry provides an efficient method for quantifying the wealth of information seen on these maps. In this way, kinemetry can be used as an analysis tool and a step between observations and theoretical modelling.

3 The method

In this section we present the details of the kinemetry method which exploits the high degree of symmetry observed in early-type galaxies. The errors are treated in more detail in Section 4.

3.1 Harmonic expansion

Fourier analysis is the most straightforward approach to characterise any periodic phenomenon. The periodicity of a kinematic moment can easily be seen by expressing the moment in polar coordinates: $K(x, y) \rightarrow K(r, \theta)$. The map $K(r, \theta)$ can then be expanded as follows to a finite number $(N + 1)$ of harmonic terms (frequencies):

$$K(r, \theta) = a_0(r) + \sum_{n=1}^{N} c_n(r) \cos[n(\theta - \phi_n(r))]. \quad (4)$$

The main advantages of this approach are: (i) linearity at constant r, and (ii) no *a priori* assumptions about the kinematic maps of the observed galaxy.

Choice of the centre and geometry of the expansion is somewhat arbitrary. We fix the centre of the polar coordinate grid at the central intensity peak in the nucleus of the galaxy, which is usually well-defined in early-type galaxies. We assume this point corresponds to the gravitational potential minimum.

We perform the expansion along a set of concentric circular annuli although in principle any geometry can be used. The main advantage of circles is that they do not introduce any *a priori* assumption about the structure of the kinematic maps (or the underlying galaxy potential). Throughout this paper we use circles to explain the basic features and properties of the kinemetric expansion, but in Sections 3.2 and 4.5 we consider expanding along elliptical annuli, with its specific application to velocity maps only.

In practice, we rewrite eq. (4) in the form:

$$K(r, \theta) = a_0(r) + \sum_{n=1}^{N} \left[a_n(r) \cos n\theta + b_n(r) \sin n\theta\right], \quad (5)$$

where the coefficients a_n, b_n are determined by a least-squares fit using singular value decomposition with a basis $\{1, \cos\theta, \sin\theta, ..., \cos N\theta, \sin N\theta\}$. The amplitude and phase coefficients (c_n, ϕ_n) of eq. (4) can be easily calculated from the a_n, b_n coefficients:

$$\begin{aligned} c_n &= \sqrt{a_n^2 + b_n^2}, \\ \phi_n &= \arctan\left(\frac{b_n}{a_n}\right). \end{aligned} \quad (6)$$

In addition to measurement errors, there are two effects which limit the reliability with which coefficients in the expansion can be determined: (i) the absolute number of points sampled along the annulus, and (ii) the regularity with which these points sample the annulus as a function of angle, θ. Figure 1 shows an example of these effects

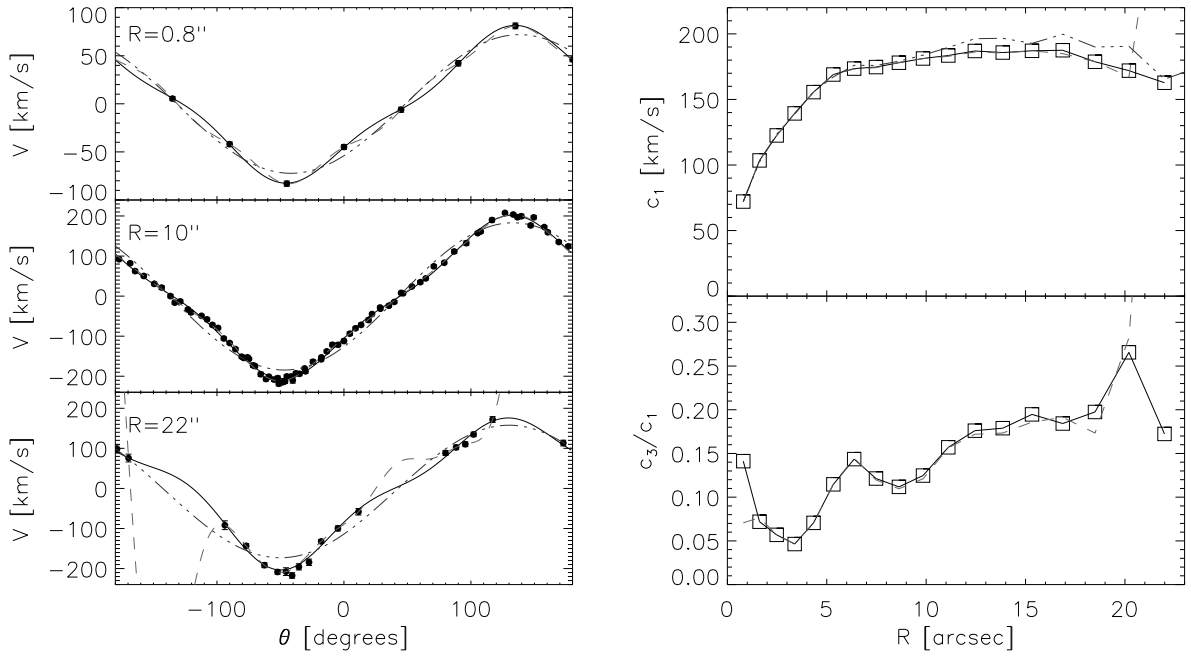

Figure 1 — Examples of kinematic profiles and kinemetric coefficients for the E4 galaxy NGC 2974 as observed with SAURON. Top left panel: the kinematic profile of the innermost annulus ($r = 0.''8$). Second left panel: the kinematic profile of an annulus at $r = 10''$ from the centre. Third left panel: the kinematic profile of an outer annulus ($r = 22''$). In these panels, the observed data are indicated by field symbols. The 1σ error bars are generally smaller than the symbols. The solid line is the fit to the data using $n_{\max} = 4$ terms. The dashed line is the fit using $n_{\max} = 7$ terms. The dash-dotted line is the fit using $n_{\max} = 2$ terms. Top right panel: the amplitude of the c_1 coefficient from the kinemetric expansion of the full velocity map of NGC 2974. Open symbols and solid line were obtained using $n_{\max} = 4$ terms in the expansion, while the dashed line using $n_{\max} = 7$ and dash-dotted line using $n_{\max} = 2$ terms. The bottom right panel: c_3/c_1 coefficient ratio from the two expansions: solid symbols and solid line for $n_{\max} = 4$ terms and dashed line for $n_{\max} = 7$ terms.

and how they limit the number of terms which can be reliably fitted to the given kinematic profile[1]. The figure is based on the observed SAURON velocity map of NGC 2974 shown on Fig.9 and described in more details in Chapter 5 of this thesis. In order to prescribe the number of terms for the expansion we impose the condition that the corresponding half-wavelength of the highest term in the expansion has to be longer than the maximum angular distance between the data points. This can be expressed by a simple relation: $n_{\max} < \pi/\Delta\theta$, where $n_{\max} = N + 1$ is the maximum number of terms used in the expansion and $\Delta\theta$ is the size of the largest distance between the data points in the kinematic profile.

At small radii (top panel in Fig. 1), the annulus intersects only a few evenly-spaced points, and $n_{\max}$ is correspondingly small (in this example $n_{\max} = 4$). At intermediate radii, (the second panel in Fig. 1), the kinematic profile is well sampled allowing more

[1]In this study we use the term "kinematic profile" to describe the variation in the value of a kinematic moment along annuli extracted from maps.

higher-order terms. At large radii (the third panel in Fig. 1), the annulus can include regions without data (sampling beyond the edge of the map), creating "holes" in the kinematic profile. The angular size of the holes limits the number of terms that can be used for the expansion (in this example $n_{\max} = 2$).

In the right panels of Fig. 1 we show the dominant odd terms, c_1 and c_3 of the harmonic expansion. The different lines correspond to the different number of terms used in fitting the kinematic profiles on the first three panels. The dashed-dotted line corresponds to $n_{\max} = 2$. These two terms alone are clearly not sufficient to fit the data. Adding more terms will increase the accuracy of the reproduction of the kinematic moment, but if too many are added, the discreteness effects will become important. The dashed line corresponds to $n_{\max} = 7$ which is well justified at intermediate radii, but in the central annulus and in the annuli at large radii ($r > 20''$), it does not satisfy the relation for maximum number of terms used in the expansion.

To combat the effects of sampling, the Fourier expansion in kinemetry is therefore performed on concentric annuli of increasing width. In general, this is the consequence of the rapidly falling signal-to-noise ratio of spectra as one goes away from the centre. The kinematic maps are necessarily binned (e.g. using adaptive Voronoi binning (Cappellari & Copin 2003) as in the presented examples), and as the bins typically increase in size with radius, the area of the annuli in which the kinematic values are selected have to increase as well to uniformly sample the kinematic profile. However, by increasing the bin size, one loses the spatial resolution and the final size of the annuli is a compromise of these two effects. We made a specific choice for the SAURON data, where the width, Δr, of a given annulus, j, is given by the expression $\Delta r_j = s \times q^{j-1}$. Here, s corresponds to the size of the smallest spatial element ($0.''8$ for SAURON), and q is a scale factor such that $\Delta r \approx 2''$ at a radius of $25''$

It should be noted that the number of terms required in the expansion depends also on the purpose of the expansion, which can be to reproduce the map in detail using a large number of terms (possibly enforcing a symmetry, as in Section 4.4) or to extract a small number of coefficients to describe the main features of the map and obtain a low-order approximation to the galaxy highlighting the key terms.

3.2 Expansion along elliptical annuli

In the previous section we discussed the kinemetric expansion of kinematic maps along circular annuli which bring no assumptions about the galaxy. However, certain physical insight for the choice of the shape of the annuli may be well justified, as in the case of surface photometry, or the analysis of velocity fields of ionised gas discs. In this section, we turn in more detail to the alternative approach of expansion along elliptical annuli. The kinemetric formalism described above remains unchanged and only the selection of the data points changes from circular to elliptical annuli.

Surface photometry of early-type galaxies has the obvious choice to expand along elliptical isophotes of the light distribution. The azimuthal surface-brightness profile at a certain radius is fitted by an ellipse and the possible deviations are represented by higher-order terms of a harmonic series. The existence and amplitude of the higher-order terms quantify the deviations of the ellipses, which have physical meaning and describe the shape of the isophotes relative to the best-fitting ellipse (e.g Lauer 1985;

Jedrzejewski 1987; Bender 1988).

Observed velocity maps of disc galaxies can be well fitted by circular motion. A standard approach of the tilted ring method (Begeman 1987) in the analysis of the velocity maps of HI, CO and Hα discs is to decompose them in a number of separate rings. Each ring is then described by six parameters: the centre coordinates, position angle, inclination, systemic velocity and circular velocity. A harmonic analysis of the rings can be performed, characterising the higher-order deviations from the pure circular motion (Franx et al. 1994; Schoenmakers et al. 1997; Wong et al. 2004).

Kinematic maps of early-type galaxies, having different symmetries and not necessarily being created by stars moving in a disc, do not offer such simply motivated geometries for the expansion. On the other hand, since their light distribution is elliptical it is reasonable to assume that an expansion along ellipses will have some advantages over the expansion along the circles. The choice of the actual ellipticity is somewhat arbitrary. For example, it is possible to expand along the galaxy isophotes or along ellipses that correspond to projected circles. In the first case, one follows the photometry and probes regions of the same projected surface brightness; while in the second case, one samples locations with equal intrinsic radii. In the second case, however, it is necessary to assume an inclination for the galaxy, which is usually difficult to estimate. Also, assuming a constant ellipticity for the whole kinematic map may not be justified.

Let us assume that the velocity maps of early-type galaxies are created by stars moving on circular orbits in thin discs. Following the tilted-ring approach, we can then divide a velocity map into a number of separate rings. The extracted velocity profile is fitted with a simple cosine function:

$$V(R, \theta) = V_0 + V_C \cos\theta, \tag{7}$$

where R is the mean radius of the ring in the plane of the galaxy, V_0 is the systemic velocity, V_C is the circular velocity not corrected for the inclination and θ is the azimuthal angle in the plane of the galaxy, which is related to the axial ratio q of the ring's major and minor axes, and is measured from the kinematic position angle of the map. Varying the axial ratio, one can find the ring whose velocity profile is the most similar to the circular velocity of a disc, with radius R and inclination $\cos i = q$. In other words, the axial ratio defines the ellipse on the sky, $q = 1 - \epsilon$, with ellipticity ϵ, which corresponds to a circle in the plane of the galaxy, describing the orbits of stars in the disc. These independent rings are then analysed by means of harmonic expansion. This approach effectively minimises the higher-order terms. If the assumption that the investigated velocity maps are similar to disc velocity maps is satisfied, then it is to be expected that the higher-order terms will be negligible. Sections 4.5 and 5.3 present an application of this modified kinemetry approach on model and observed velocity maps, respectively.

4 Kinematic parameters and their meaning

Kinemetric analysis is possible for all measured kinematic moments. The properties and meaning of the kinemetric coefficients will differ depending on the underlying symmetry of the analysed map. The influence of the map symmetry on the coefficients can be predicted and compared to the obtained kinemetric values. On the other hand,

assuming a symmetry one can obtain the properties of the map by effectively filtering the noise in the data. In this section we characterise the kinemetric coefficients for odd and even kinematic moments, present the filtering capabilities of kinemetry and discuss kinemetry along ellipses.

4.1 Model galaxy

We constructed a model galaxy to demonstrate the application of kinemetry. The model is axisymmetric with a distribution function which depends only on the energy and one component of the angular momentum. The model was constructed using the Hunter & Qian (1993) contour integration method and following the prescriptions of Emsellem et al. (1999) to resemble the SAURON observations of NGC 2974: surface-brightness distribution, kinematic observations, inclination, mass-to-light ratio and central black hole mass. The distribution function of the model yields the full LOSVD from which the observable kinematics can be extracted. This was done on a large $100'' \times 100''$ field by fitting a Gauss-Hermite series (V, σ, h_3 and h_4) to spatially binned data which resemble typical SAURON observations. In order to mimic the real observations, we also assigned the typical error of the SAURON observations to each model observable. These errors were used to add intrinsic scatter to the noiseless model data by means of a Monte Carlo realisation. Further details on the construction of the model galaxy and its kinematics are given in Section 5.1 of Chapter 5 of this thesis.

This model is an example of an axisymmetric galaxy, with mirror-(anti)-symmetric kinematic maps. Although kinemetric analysis of a more complicated model is also possible (and equally straightforward), here we present a simpler example to clearly quantify the main properties of the kinematic moment maps and the results of kinemetry.

4.2 Odd kinematic moments

In a Gauss-Hermite parameterisation of the LOSVD, the first two odd moments are the mean velocity V, and the Gauss-Hermite coefficient h_3. The maps of these moments look different and have different interpretations, but have the same underlying symmetry. Generally, maps of odd moments show *point-anti-symmetry*. Imposing the point-anti-symmetry condition (eqs. 2–3) on the terms of the kinemetric expansion (eq. 4), for the odd moments of LOSVD one has:

$$\mu_o(-x,-y) = -\mu_o(x,y) \quad \Rightarrow \quad a_0 = c_{2n} \equiv 0. \tag{8}$$

A map with additional *mirror-anti-symmetry* (an axisymmetric case) requires also:

$$\mu_o(x,-y) = \mu_o(x,y) \quad \Rightarrow \quad \phi_{2n+1} = const \equiv \mathrm{PA}. \tag{9}$$

Therefore, one can predict that in an observed odd moment map the even terms will be considerably smaller than the odd ones, where the departures from zero are caused by noise or possible lopsidedness (departures from the assumed symmetry).

Figures 2 and 3 show the kinemetric expansion of the V and h_3 maps of the model galaxy. The errors were estimated using Monte Carlo simulations. The kinemetric coefficients were derived from 100 realisations of the moment map, where the moment's value in each spatial bin was taken from a Gaussian distribution with the mean of the original moment and standard deviation given by the error assigned to the moment in the bin. Each realisation of the map was expanded using kinemetry providing a distribution of values from which we estimate the 1σ confidence limit.

The zeroth-order term, a_0, measures the mean level of the map. For the first kinematic moment, this is equivalent to the systemic velocity of the galaxy. In the case of the model velocity field, the systemic velocity was zero by construction, and in an observed galaxy, a_0 will be non-zero. However, if the systemic velocity is properly subtracted (as it was assumed in eq. 8), a_0 will be zero. Alternatively, using the kinemetric expansion it is possible to determine a reliable systemic velocity using the information of the whole velocity map. In the case of the observed h_3 maps, which have mean level equal to zero by construction, a_0 will be small, and like other even terms, consistent with zero.

The coefficient c_1 gives the general shape and amplitude of the odd moment map and is always the dominant term. Hereafter, we normalise the higher coefficients, $c_{i>1}$, in the kinemetric expansion of the velocity map by c_1, to simplify the comparison between the terms.

The first-order correction is given by the next odd term, c_3. This term can be named the *morphology* term because it describes most of the additional geometry of the map. Generally, the first two odd terms are enough to describe the velocity map, although the kinemetric expansion can include higher terms as well, c_5 and even c_7. In Fig 2 and 3 we plot the c_5 term for completeness. Although in some instances this term can become significant (around $20''$ in this case), it is generally very small, being at the level of noise in the data.

Connected to the amplitude terms are the corresponding phase terms, ϕ_n. They determine the orientation of the map, but their contribution depends on the relative strength of the amplitude terms. The first phase coefficient, ϕ_1, gives the mean position angle of the velocity map (measured from the horizontal axis, $\theta = 0$). We name it the *kinematic angle*. The angle that ϕ_1 measures is the position angle of the maximum c_1 term. This is, in general, slightly different from the positions of the maxima on the map, which are also influenced by the contribution from higher-order terms. However, it does give the global orientation of the map at a given radius to a good approximation and can be used to describe the symmetry of the map (Section 5.1).

The angle ϕ_3 is the phase angle of the third harmonic: the next significant term. For a small amplitude of c_3, its contribution to the overall orientation will be small, and the position of the maximum velocity will be given accurately by $\theta_{max} = \phi_1$. For an axisymmetric galaxy ϕ_3 will have specific values, as we will see in Section 5.1.

The error bars plotted on Fig. 2 and 3 (as well as on Fig. 4 and 5 of the next section) are typical for the SAURON observations of the nearby galaxies (Emsellem et al. 2004). As expected, due to the discreteness, they are larger at small and large radii where the sampling and edge effects play an important role. In the case of the velocity maps, at intermediated radii with dense sampling of kinematic profiles, the typical intrinsic

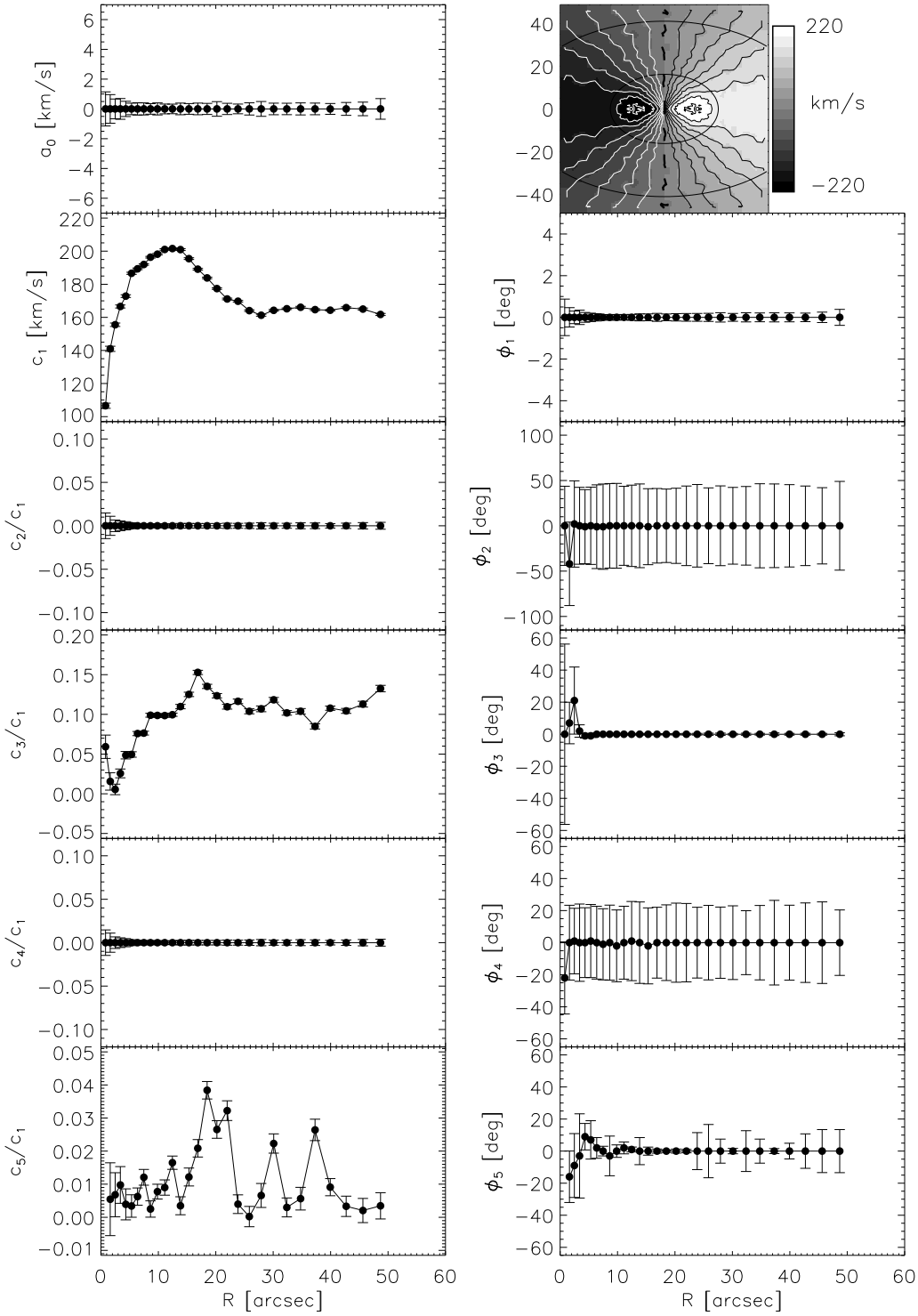

Figure 2 — Kinemetric expansion of the velocity map of the model axisymmetric galaxy. Panels of the left column show the amplitude coefficients of the kinemetric expansion (from top to bottom): a_0, c_1, c_2/c_1, c_3/c_1, c_4/c_1 and c_5/c_1. The velocity map is presented in the upper right, while other panels in the right column show the corresponding phase angles (from top to bottom): ϕ_1, ϕ_2, ϕ_3, ϕ_4 and ϕ_5. The relatively large errors to the even phase angles are not significant because the associated amplitude is zero.

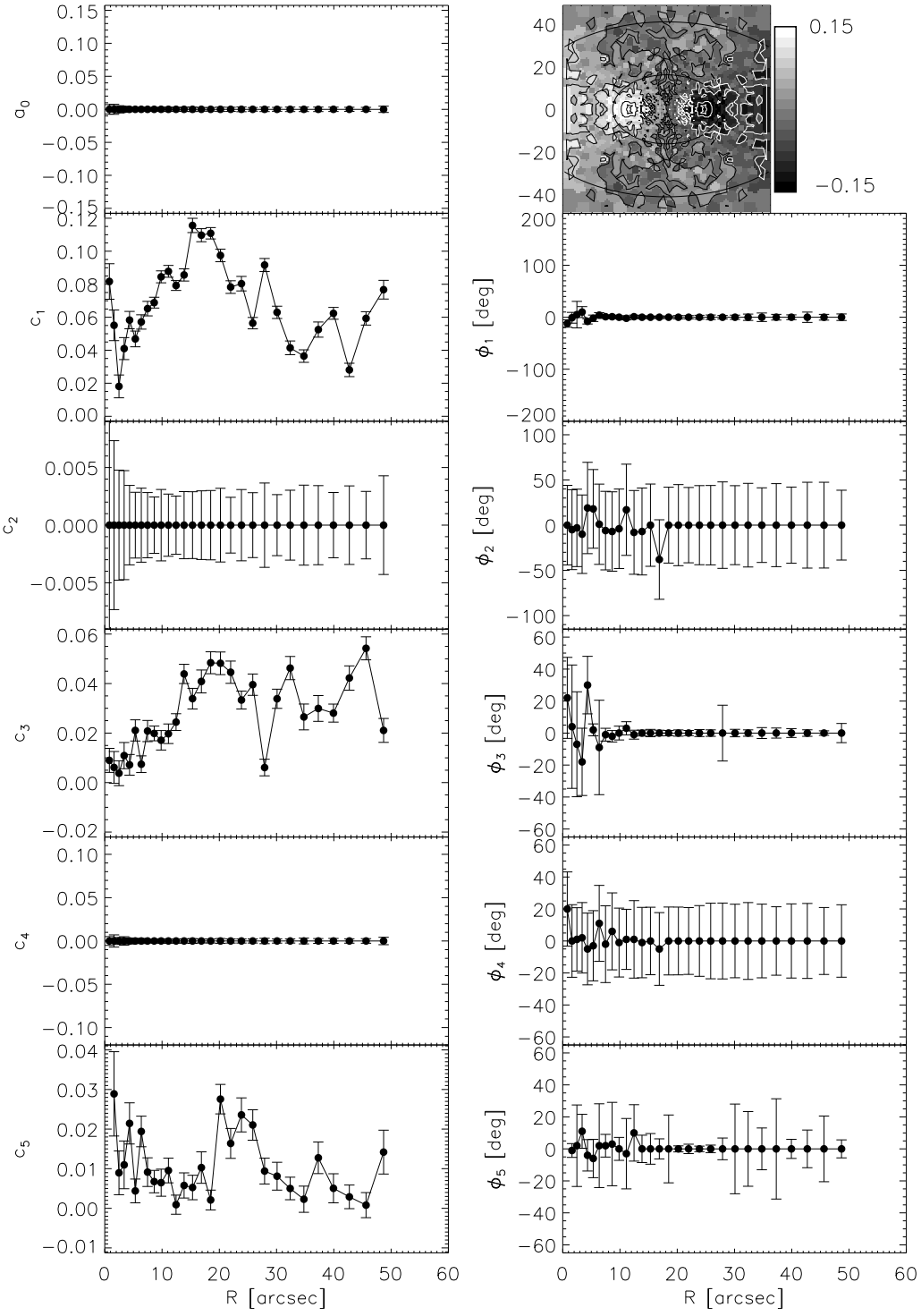

Figure 3 — Kinemetric expansion of the h_3 map of the model axisymmetric galaxy. Panels of the left column show the amplitude coefficients of the kinemetric expansion (from top to bottom): a_0, c_1, c_2, c_3, c_4 and c_5. The h_3 map is presented in the upper right panel, while the other panels show the same phase angles as in Fig 2, but for the h_3 map.

errors (not accounting for systematics) for the c_1 and c_3 coefficients are $0.5\,\mathrm{km\,s^{-1}}$ and $0.6\,\mathrm{km\,s^{-1}}$, respectively; and for the ϕ_1 and ϕ_3 phase angles are 0.5° and 1°, respectively. The larger errors on the phase angles of the even terms can be explained by the near-zero values of the corresponding amplitude coefficients. The same effect is visible for the phase angles of the higher-order odd terms, when they have near-zero values. Similar, but somewhat higher values are seen for the errors on the kinemetric terms of higher-order kinematic moments (σ, h_3, h_4).

The same description can be assigned to all terms of the kinemetric expansion of h_3 maps. The values of the amplitude coefficients c_i are much smaller for the h_3 moment ($c_i < 1$), and the rescaling of the higher terms with the dominant term is not very useful. The h_3 map is noisier than the mean velocity map. This is reflected in the recovered errors of the coefficients, which are somewhat larger, even for the odd terms, than in the case of the mean velocity map. The typical intrinsic errors of kinemetric expansion of h_3 maps for the c_1 and c_3 coefficients are 0.04 and 0.005, respectively; and for the ϕ_1 and ϕ_3 phase angles are 3° and 4°, respectively.

4.3 Even kinematic moments

The even terms in the standard parametrisation of the LOSVD are the velocity dispersion σ, and the Gauss-Hermite coefficient h_4. In many ways, analysis of the even moments is analogous to that for the odd moments, taking the proper parity into account. The maps of even moments show *point-symmetry* which translates to the terms of the kinemetric expansion as:

$$\mu_e(-x,-y) = -\mu_e(x,y) \quad \Rightarrow \quad c_{2n+1} \equiv 0. \tag{10}$$

A map with additional *mirror-symmetry* requires:

$$\mu_e(x,-y) = \mu_e(x,y) \quad \Rightarrow \quad \phi_{2n} = const \equiv \mathrm{PA}. \tag{11}$$

As anticipated, the odd kinemetric terms are expected to be consistent with zero on the observed maps of even moments. This is clearly visible in Figs. 4 and 5, which show the coefficients of the kinemetric expansion of the model velocity dispersion and h_4 maps. The 1σ confidence levels shown in the figures were obtained via Monte Carlo simulations as in Section 4.2.

The dominant term of the even maps is a_0, and it describes the absolute level of the map as a function of radius. The next important term in the expansion is c_2, and it is the *morphology* term of the even moment maps. As seen in Figs. 4 and 5 this term describes more specific features of the maps. Features such as elongations along the minor axis or "bow-tie" shapes, often seen in observed velocity dispersion maps (Emsellem et al. 2004), should leave signatures in this term. Specifically, for the velocity dispersion maps the c_2 term is mostly a few percent of the dominant a_0 term, implying that these maps have near-circular symmetry, and that the choice of circles for describing these maps is a natural one.

The orientation of the morphologically distinct features are determined by the phase angles of the amplitude coefficients. When there is a feature with a specific angular dependence, e.g. an oval elongation along the major axis, the position angle of the feature

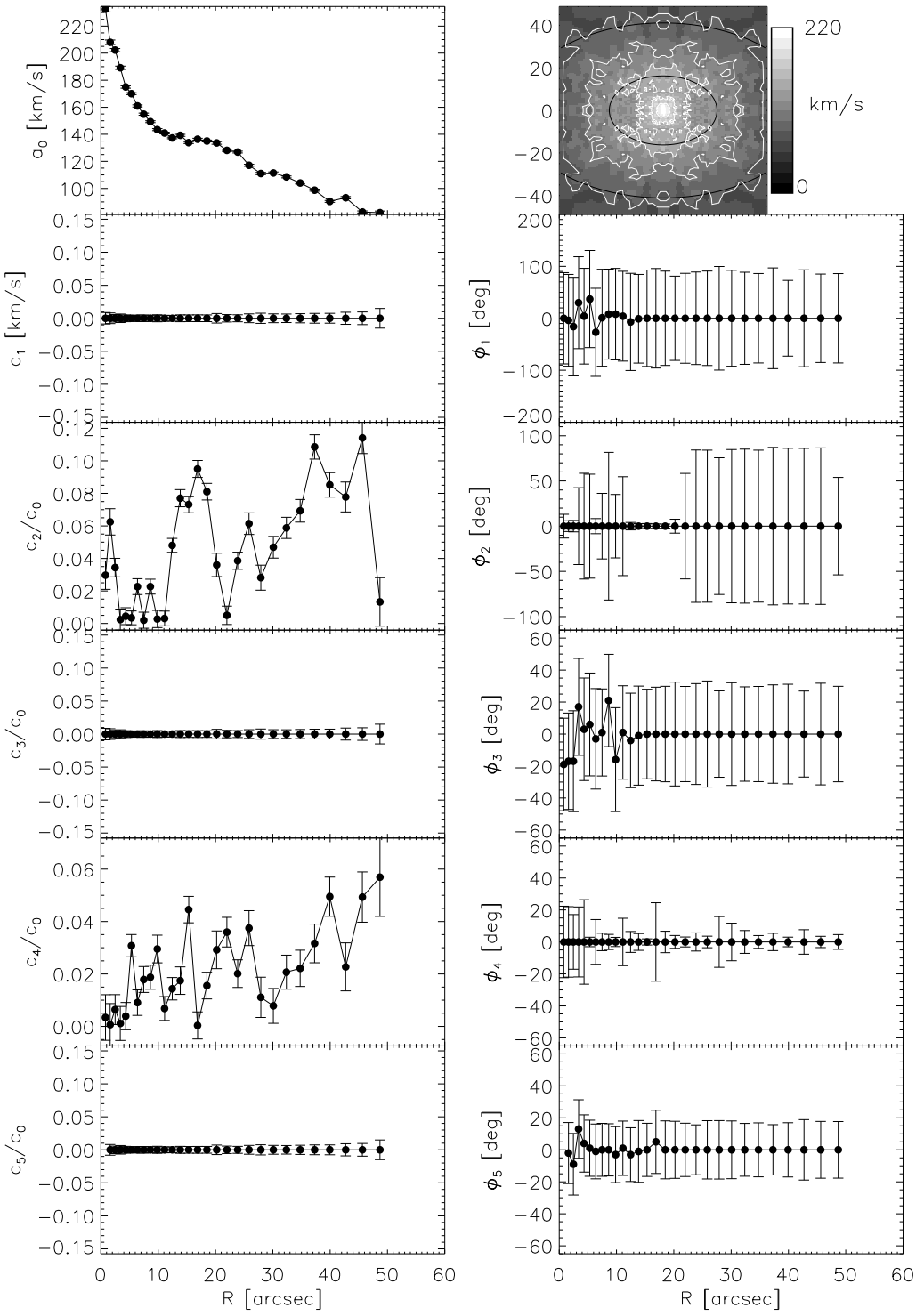

Figure 4 — Kinemetric expansion of velocity dispersion map of the model axisymmetric galaxy. Panels on the left column show amplitude coefficients of the kinemetric expansion (from top to bottom): a_0, c_1/a_0, c_2/a_0, c_3/a_0, c_4/a_0 and c_5/a_0. The velocity dispersion map is presented in the upper right, while other panels in the right column show the same phase angles as in Fig 2, but for the velocity dispersion map.

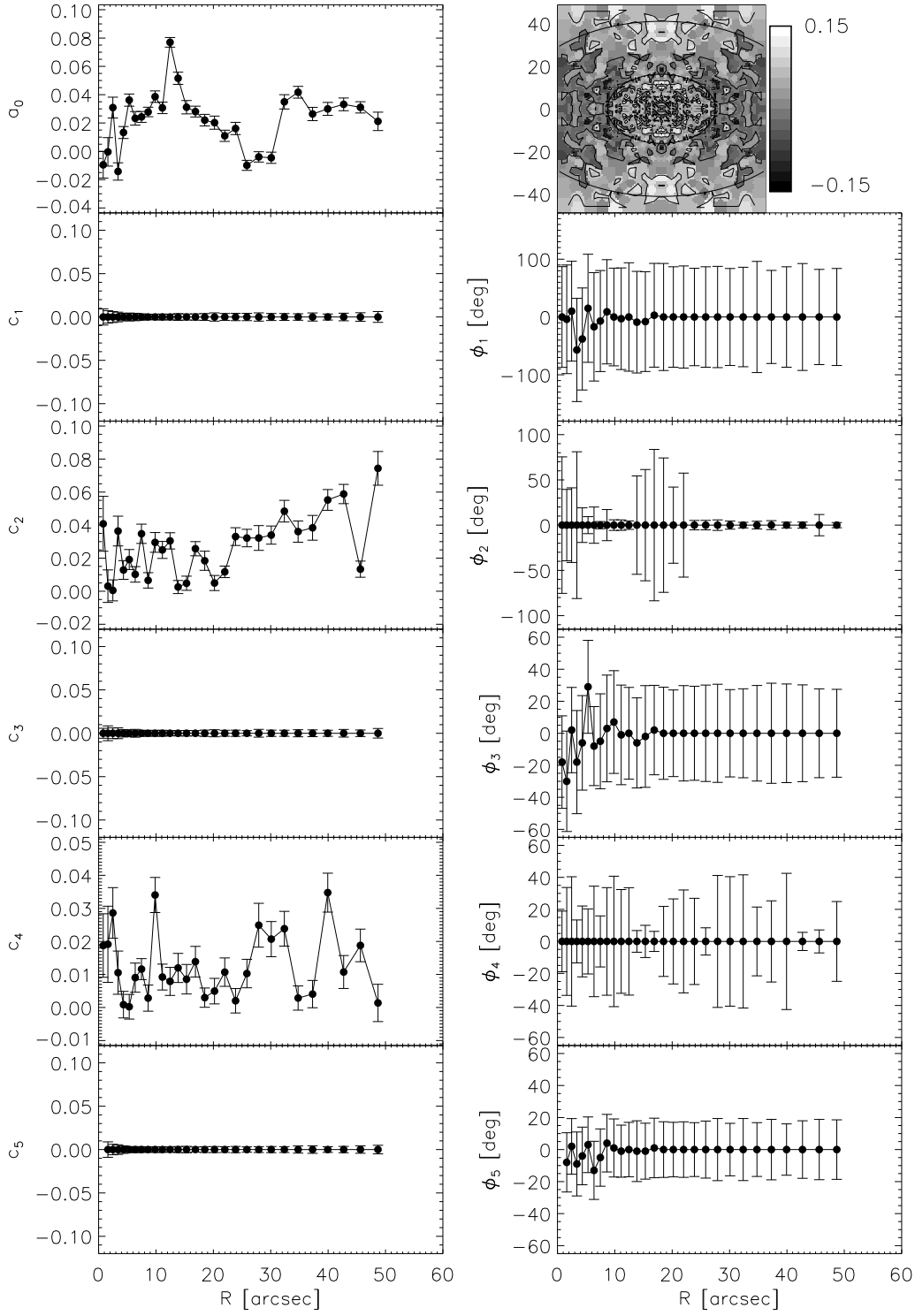

Figure 5 — Kinemetric expansion of the h_4 map of the model axisymmetric galaxy. Panels on the left column show amplitude coefficients of the kinemetric expansion (from top to bottom): a_0, c_1, c_2, c_3, c_4 and c_5. The h_4 map is presented in the upper right panel, while the other panels show the same phase angles as in Fig 2, but for the h_4 map.

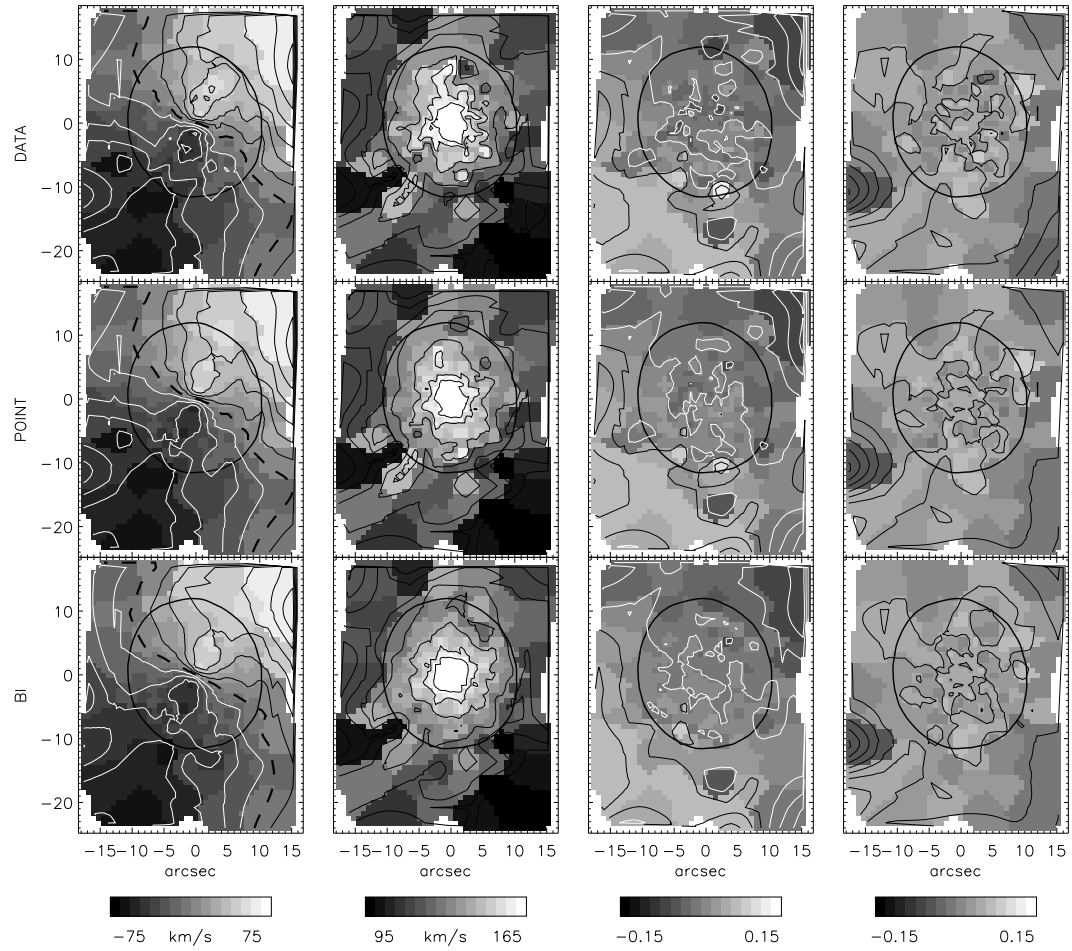

Figure 6 — An example of kinemetric filtering on kinematic maps of the galaxy NGC 474. Rows from left to right: mean velocity V, velocity dispersion σ, and Gauss-Hermite moments h_3 and h_4. Columns from top to bottom: data, symmetrised data applying additional *point-(anti)-symmetric* condition (eqs. 8 and 10), data symmetrised applying additional *mirror-(anti)-symmetric* condition (eqs. 9 and 11). The overplotted kinematic contours were obtained by interpolation between the bin generators and extrapolation to the edge of the maps.

is given by the ϕ_2 phase angle of the c_2 term. The phase angles of the odd terms, whose amplitude coefficients are zero, have large errors, while the errors of the even phase angles are generally smaller, although still high at certain radii, suggesting there is no preferred direction of the features on the example maps. The typical intrinsic errors for kinemetric expansion of the velocity dispersion maps are: $0.9\,\mathrm{km\,s^{-1}}$ and $1.1\,\mathrm{km\,s^{-1}}$ for a_0 and c_2 coefficients, respectively, and 3° for the ϕ_2 phase angle in the region where the phase angle is well constrained. Similarly, for the expansion of the h_4 map we obtained errors of 0.005, 0.006 and 5° for a_0, c_2 and ϕ_2, respectively.

4.4 Filtering

Kinemetry can also be useful as a powerful *filter* of two-dimensional kinematic maps. As already mentioned above, if the number of terms in the expansion is small, the

map will be smoothed, taking away the higher-order harmonics from the data, which may be caused by noise. However, kinemetry offers some other more specific filtering, which makes assumptions of the underlying symmetries in the kinematic maps.

Following eqs. (8) and (9), one can filter a kinematic map by fixing certain terms in the expansion to zero or to a constant value. Requiring *point-anti-symmetry* in the kinemetric expansion for odd maps implies fixing the even terms to zero (in case of an even map, the odd terms are set to zero).

Similarly, a more strict requirement that all non-zero phases are set to a constant value will produce *mirror-(anti)-symmetric* maps. This symmetry removes twists of the kinematic angle, creating what is sometimes called a *bi-symmetric map*. These filtering criteria may also be applied to extract the relevant coefficients from maps with noisy data.

Figure 6 gives an example of filtering, applied to the first four observed moments of the LOSVD for SAURON observations of NGC 474 (Emsellem et al. 2004). The kinematic maps of this galaxy are consistent with *point-(anti)-symmetry* and, applying this symmetry condition to the kinemetric expansion, removes much of the noise from the data. However, in the following example, we set all (non-zero) phases to the median value of the measured kinematic angle ($\approx 60^\circ$), enforcing additional *mirror-(anti)-symmetry*, with which the galaxy kinematics are clearly not consistent. The results are axisymmetric kinematic maps (no kinematic twists), that, however, do not correspond to the real galaxy, but show the full filtering power of kinemetry.

A draw-back of filtering such integral-field data with kinemetry comes from the nature of the spatial bins. Generally, the bins are not symmetrically distributed around the symmetry axes. Kinemetric filtering works in annuli and if the bins are not uniformly distributed in the annuli, it will not be possible to find symmetric pairs of bins in all quadrants of the map and properly enforce the symmetry (e.g. $K(-x,-y) = -K(x,y) = -K(x,-y) = K(-x,y)$). A way out is to interpolate the binned data on a regular grid and then symmetrise using kinemetry, although the best way of symmetrising the maps of the kinematic moments is to impose symmetry during the extraction of the kinematics from the observed data cube spectra.

4.5 Expansion of velocity maps using kinemetry along ellipses

At this point we turn again to the special case of kinemetry along ellipses. In Section 3.2 we suggested that the tilted-ring approach to the velocity maps of early-type galaxies, although not physically founded, might give a better insight in the structure of maps. Here we show an example of the kinemetric expansion of the velocity map of the model galaxy discussed in Fig. 2 along ellipses best-fitting ellipses following the prescription of Section 3.2.

We performed the expansion up to the third odd term (c_1, c_3 and c_5), where the c_1 term is by construction identical to V_C from eq. (7), while the higher-order terms describe the deviations of the velocity map from the projected circular motion. The result is shown in Fig. 7. The first panel of the figure shows the axial ratio of the elliptical rings used in the expansion. In the inner few arcseconds this ratio changes and then drops to a constant value of relatively *round* value for the axial ratio of about $q = 0.7$. Strikingly, the higher-order terms, plotted on the lower panels, are negligible, their

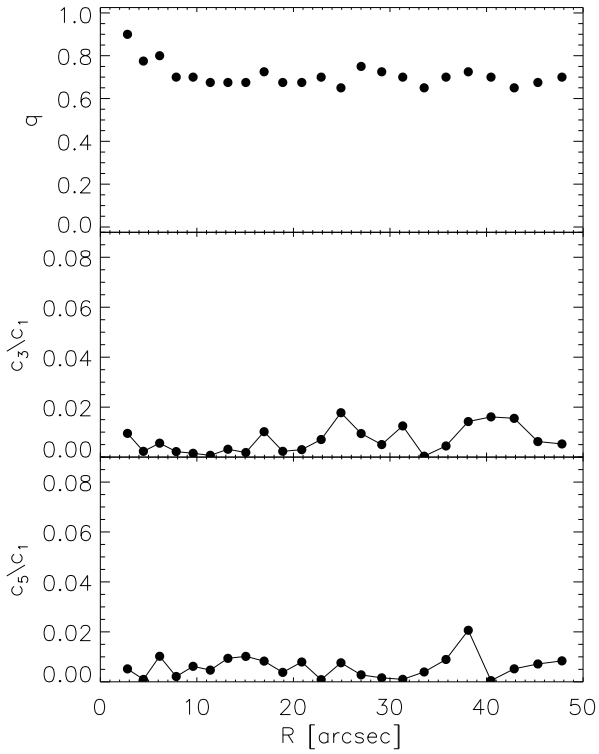

Figure 7 — Terms of kinemetric expansion of the velocity map of the model galaxy along ellipses. From top to bottom: axial ratio of the best-fitting ellipse, and the ratio of the c_3/c_1 and c_5/c_1 terms which measure the deviation from the circular velocity assuming the velocity map was generated by stars moving along circular orbits in a disc. The deviations are below the 1% level. See text for details.

contribution being mostly below the 1% level. This shows the power of this approach, which can describe a velocity field with basically two parameters: the axial ratio of the adopted ellipse and the first term of the harmonic expansion.

The underlying assumption of this application of kinemetry is that the velocity maps of early-type galaxies are created by stars moving along circular orbits in a thin disc. This, generally, is not true, and our intention here is only to qualitatively compare the observed velocity maps of spheroidal systems with those of thin discs. In the example shown in Fig. 7, the higher-order terms are very small and the velocity map of the model early-type galaxy seems to be consistent with a velocity map of an inclined disc. Our comparison stops here, but it is an interesting finding, worth more detailed investigation (see Section 5.3). Along the same lines, the axial ratio, q, from Fig. 7, does not imply the intrinsic inclination of the galaxy. It can, however, be used to categorise the velocity maps: velocity maps with small q are *flat* while velocity maps with high q are *round*.

5 Application

In this section we consider the ability of kinemetry to quantify the underlying symmetries of kinematic maps of observed galaxies, as well as give examples of kinemetry along ellipses for three early-type galaxies. For this purpose we focus on the velocity maps.

5.1 Prescription for axisymmetry

Two-dimensional velocity maps can be used to constrain the intrinsic shapes of early-type galaxies (Franx et al. 1991; Statler 1994b), and kinemetry can serve as a tool for extracting the necessary information from the maps. Here we consider conditions by which one can distinguish between velocity maps of axisymmetric and more general triaxial galaxies.

Axisymmetry is a special case of triaxiality, and triaxial galaxies, viewed under certain inclination can have axisymmetric appearance (e.g Stark 1977; de Zeeuw & Franx 1989). A galaxy is consistent with axisymmetry if the velocity map satisfies the following three conditions:

1. The velocity map is truly *point-anti-symmetric*, and, hence, the even terms in kinemetric expansion are zero (or negligible), as given by (8).
2. The velocity map satisfies the condition (9), where all phase angles are constant.
3. All phase angles are equal to the photometric position angle. This condition can be softened by requiring that the higher-order phase angles satisfy the relation:

$$\phi_1 - \phi_i = \frac{n\pi}{i}, \tag{12}$$

where $n \in \mathbb{Z}$ and ϕ_i is the i-th order term in the expansion.

The last condition can be easily derived considering that for an axisymmetric velocity field the position of the zero velocity curve, the curve along which the velocity is zero on the map, is orthogonal to the kinematic angle given by ϕ_1. This means that $K(r, \theta) = 0$, for $\theta = \phi_1 + \pi/2$. Neglecting the higher order terms, ($c_i > c_3$), and substituting $\theta = \phi_1 + \pi/2$ into eq. (4) one obtains the result of eq. (12).

Similarly, deviations from axisymmetry can be quantified following eqs. (4) and (12). If $K(r, \theta = \phi_1 + \pi/2) = \Delta V \neq 0$, then one finds:

$$\frac{\Delta V}{c_1} = \frac{c_3}{c_1} \sin 3(\phi_1 - \phi_3), \tag{13}$$

where we express the relation as a ratio of the dominant term in the expansion. This relation quantifies the contribution of the c_3 term due to departures from axisymmetry and can be generalised to other higher terms. In cases of large misalignments between the kinematic and photometric position angles, ϕ_1 should be replaced by the photometric PA in the above equation.

Fig. 2 shows the kinemetric expansion of a mirror-anti-symmetric velocity map and it is clear that all three conditions for axisymmetry are satisfied.

5.2 A triaxial case

In the previous section we presented the prescriptions for axisymmetry which were tested on an axisymmetric model velocity field. Here we turn to the wealth of the SAURON observations and use an observed velocity field of a triaxial galaxy, in order to show the departures from the conditions listed in the previous section. The velocity field belongs to the well studied triaxial galaxy NGC 4365. The SAURON kinematics, as

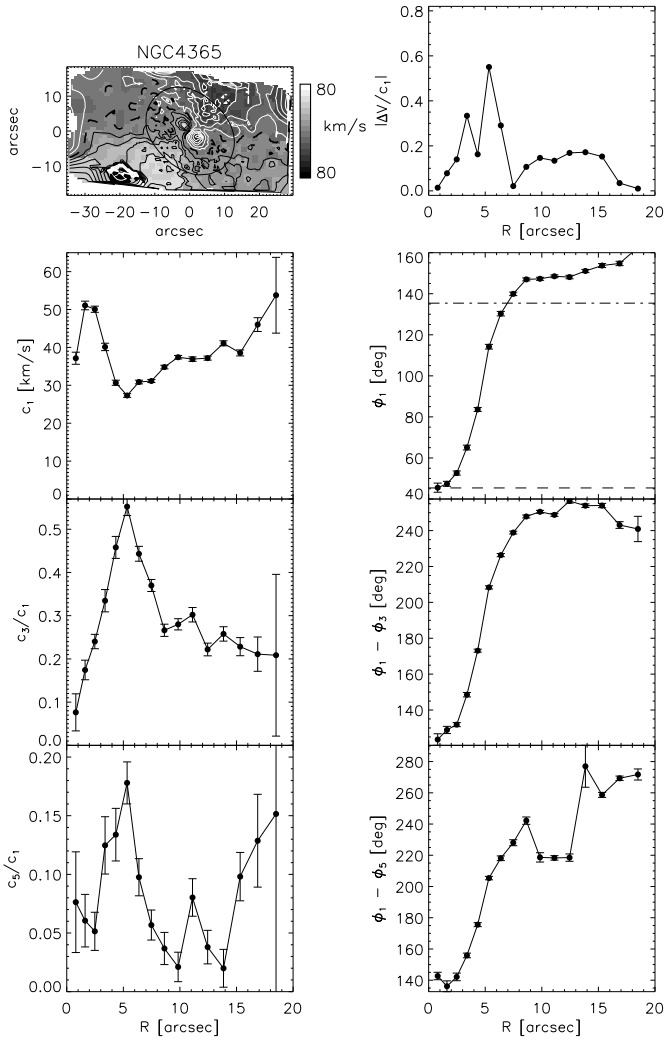

Figure 8 — Kinemetric analysis of NGC 4365. The velocity map of NGC 4365 is presented in the upper left panel. The panels in the left column show: odd amplitude coefficients: c_1, c_3 and c_5. Higher order terms are presented as fractions of c_1, the dominant term in the expansion. The first panel on the right shows the contribution of the c_3 term to non-axisymmetry. Other panels in the right column present the phase angles: ϕ_1, ϕ_3 and ϕ_5. Higher order phase angles are compared to the phase angle of the dominant terms ϕ_1 by subtraction. North is up and east to the left on the velocity map and ϕ_1 is measured east of north. Second panel on the right also shows major (lower straight line) and minor axis (upper straight line) photometric PAs.

well as the distribution of line-strengths, for this object were presented in Davies et al. (2001).

The velocity map of NGC 4365 (Fig. 8) shows a striking kinematically decoupled component (KDC) in the central 5″. The structure and shape of this component led several authors to conclude that NGC 4365 is intrinsically a triaxial body showing no figure rotation (Surma & Bender 1995; Statler et al. 2004). We performed a kinemetric analysis of the velocity map, expanding up to the fifth term (c_5). The resulting coefficients and corresponding phase angles are shown in Fig. 8.

The KDC component is clearly evident in the dominant c_1 terms as the fastest rotating component of the galaxy, with a well-defined radius. The main body of the galaxy shows increasing rotation with increasing radius, but remains a slow rotator ($V/\sigma = 0.08$, Surma & Bender 1995). The *morphology* term, c_3, is very strong, contributing up to 50% to the velocity field, and is strongest at the transition radius between the KDC and the main body of the galaxy. At larger radii, it slowly drops, but its relative contribution (about 20%) stays high. In the last extracted term, c_5, there is still considerable signal, again strongest in the transition region between the KDC and the rest of the galaxy. The contributions from the higher order terms ($c_i, i \geq 7$) are on the order of

a few per cent.

The amplitude coefficients accurately describe the map, but the phase angles are useful for the determination of departures from axisymmetry. The kinematic angle, ϕ_1, shows a clear twist of more then 100° over the map. The photometric major and minor axis PAs are overplotted on the same panel with two horizontal lines. We measured the PA on the reconstructed SAURON flux image obtained by integrating the spectra in each bin. The kinematic angle of the KDC is aligned with the major axis PA, while the main body of the galaxy rotates about an axis misaligned by about 10° from the major axis PA of the galaxy, as previously noted by Davies et al. (2001). This is a clear signature of non-axisymmetry. This conclusion is confirmed by the $\phi_1 - \phi_3$ profile, which changes in step with ϕ_1, nowhere strictly satisfying the relation (12). The contribution of the c_3 term, expressed by eq. (13), and presented in the top left panel of Fig. 8, is high everywhere, especially in the transition region between the KDC and the main body of the galaxy.

5.3 Comparison of velocity fields of early-type galaxies with velocity fields of discs

We turn again to the case of kinemetry along ellipses. Repeating the analysis from Section 4.5 we also analysed the velocity maps of three galaxies observed with SAURON as part of the SAURON survey (de Zeeuw et al. 2002). The observations and the velocity maps of NGC 524, NGC 2974 and NGC 4526 are presented in Emsellem et al. (2004). We chose these three galaxies as characteristic examples due to their shape and the pedagogical features of their velocity maps. NGC 524 is a roundish galaxy with an "open" velocity map. NGC 2974 is a fast-rotating E4 galaxy, and NGC 4526 is an S0 galaxy with a prominent embedded disc which can be also seen on the velocity map as a distinct component.

Fig. 9 presents the analysis of the three velocity maps. The analysis of the real observations with ellipses is more complicated than the analysis with circles or the analysis of the large model field (sampling issues), so, we had to rebin the velocity map to a finer grid (4 times finer). This is especially important in the centres of the field, where sampling can cause strong artifacts. The maps were also rotated such that the photometric major axes are horizontal in Fig. 9. The maps are presented above each corresponding set of kinemetric expansion terms. We summarise the main results as follows:

NGC 524 has a velocity field with high axial ratio and hence we can label it as a *round* velocity field. The higher-order terms c_3 and c_5 are small over the entire map, with a relative contribution to the circular velocity of about 2% and 1% respectively.

NGC 2974 has a mean photometric flattening of ~ 0.6 and the flattening of the velocity field corresponds to this value (expressed as axial ratio q on the figure). This velocity field is an example of a medium-flattened velocity field. The higher-order deviations from the circular velocity are smaller than in the case of NGC 524, c_3 having a relative contribution of $\approx 1\%$ and c_5 of $\approx 0.5\%$.

NGC 4526 is a more complicated map with its two kinematic components. The central disc on the velocity map is clearly visible in the inner 10″. This structure is reflected in the terms of the kinemetric analysis. The axial ratio is ≈ 0.2 in the inner 5″, while beyond that radius it is much higher and varies between 0.6 and 0.8. The velocity

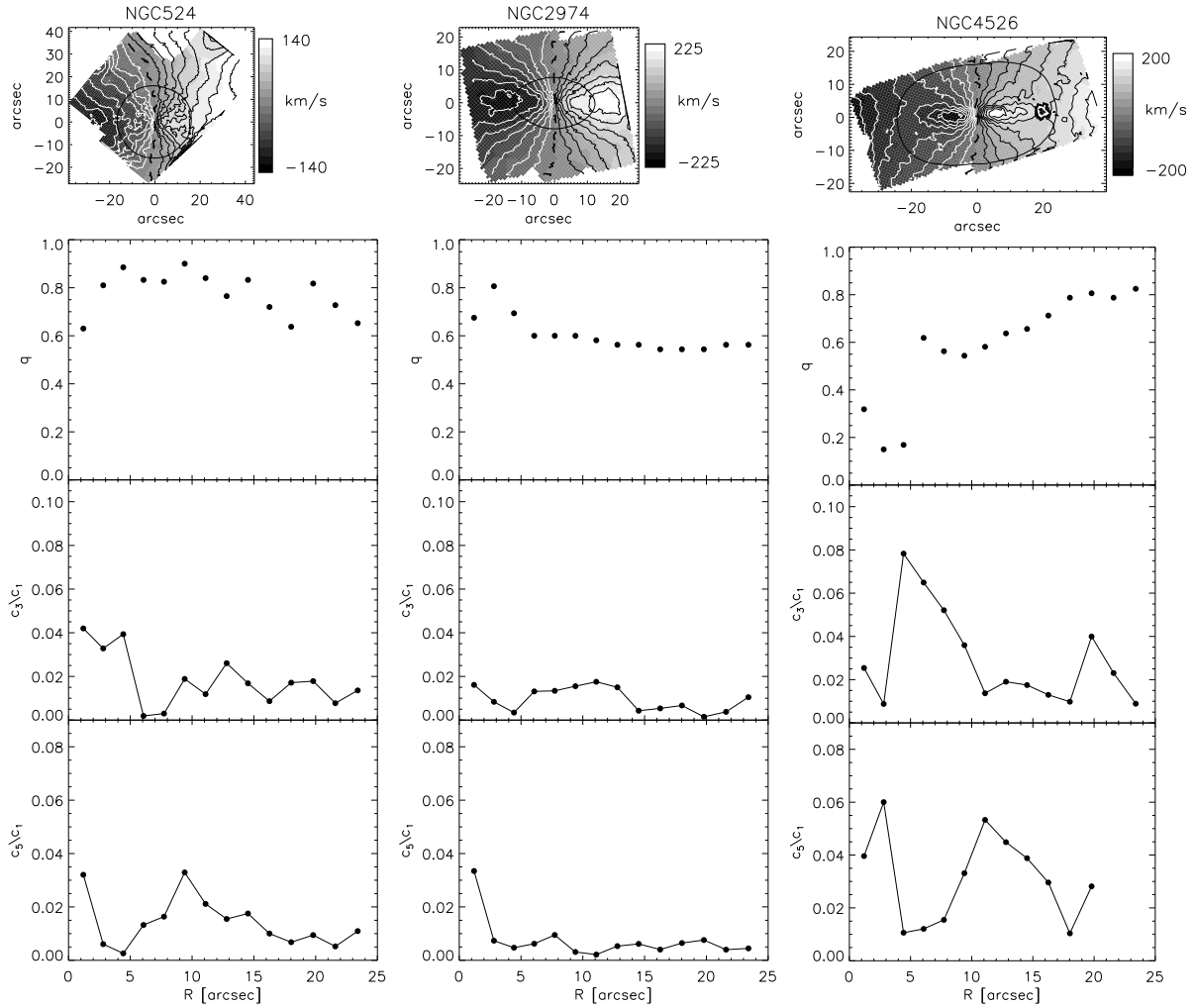

Figure 9 — Kinemetric analysis along ellipses for velocity maps of three early-type galaxies observed with SAURON. First row from left to right: velocity maps of NGC 524, NGC 2974 and NGC 4526. Second row from left to right: axial ratio q of the best fitting ellipse describing the *flattening* of the velocity field. Third and fourth rows from left to right: ratio of the terms in the kinemetric expansion: c_3/c_1 and c_5/c_1, respectively.

map in the inner few arcsec is clearly different from the rest of the map. The inner part is quite *flat*, while the outer part has more *round* features, somewhere between NGC 2974 and NGC 524. The higher-order terms are also different on this velocity map. The relative contribution of c_3 is much higher than in the two other examples (up to ~ 5 times), especially in the part where the velocity map is *flat*. The middle part of the field is more similar to projected circular motion, with a small c_3 term. Towards the end of the map, edge effects have an increasing influence on the expansion (Section 3). At radii larger than $20''$, we only used the c_3 term in expansion. The contribution of the c_5 term is smaller, but, interestingly, not negligible in the middle part of the map.

The similarities of the velocity maps of early-type galaxies with disc velocity maps are striking. It might be the case that the three investigated galaxies have a strong disc contribution which dominates the appearance of the velocity map, while the specific

features are visible from the small departures of the higher terms. Similar result was also seen in the model velocity field, which coressponds to a model galaxy with no disc component. In analogy with photometry, the deviations of the higher-order terms are also on the order of a few percent. This warrants a detailed study of a larger sample of two-dimensional velocity maps, such as the 48 SAURON galaxies from Emsellem et al. (2004).

6 Conclusions

We have presented a general method for analysing and describing two-dimensional maps of the kinematic moments observed with integral-field spectrographs. The method is based on the harmonic expansion of velocity maps. It is particularly useful for describing the maps of kinematic moments of early-type galaxies. We call our method *kinemetry*.

Kinemetry is a straight-forward Fourier expansion of two-dimensional maps. Using the specific properties of the kinematic moments (symmetries) it can be used as a powerful filter to the data. The results of kinemetry, the coefficients of the harmonic expansion, can be used to parametrise trends and detect properties of galaxies. Maps of odd kinematic moments are described only by the odd terms in the expansion. Similarly, maps of even moments are described only by the even terms.

In the case of odd maps, the first term is the most dominant term and gives the overall shape of the map (the zeroth term can exist for velocity maps and gives the systemic velocity). The third term describes the additional morphological shapes. In some galaxies, higher terms can also be significant, although usually the first and third term reproduce all important features of the map. The phase angle of the first term gives the orientation of the map and it is called kinematic angle. Higher-order phase angles are useful in detecting small departures from axisymmetry.

In the case of even maps, the zeroth term is the dominant term and it describes the global shape of the map. The next important terms which describes the morphology of the map in more detail, is the second term in the expansion. The zeroth term does not have a phase angle, and the orientation of the features of the maps are given by the phase angle of the second term.

The measured values of the kinemetric coefficients can be used to detect departures from axisymmetry in the observed maps, and in this way, to quantify the intrinsic shape of the galaxy. The necessary requirement for a velocity map to be consistent with axisymmetry is that the even terms in the expansion are consistent with zero and that the kinematic angle is constant and equal to the photometric position angle. We present a diagnostic tool for determining the consistency of velocity maps with axisymmetry using the phase angles of the first two odd terms as well as quantifying the departures from an axisymmetric velocity map. We apply this method to the triaxial galaxy NGC 4365 as an obvious case of a non-axisymmetric object, with a decoupled component and a strong kinematic twist.

Circular rings are the most natural choice for expansion, because they are simple, general and can be uniformly used on maps of all kinematic moments. In some cases, like for the velocity maps, it is necessary to expand the maps to a relatively large num-

ber of terms (up to c_5 or even c_7 of the harmonic expansion judging from a preliminary study of SAURON velocity maps (Emsellem et al. 2004)). In other cases, e.g. for the velocity dispersion maps only a small number of terms (up to c_2) are needed when the expansion is performed along circles. We note that the maps of line-strengths, which resemble the maps of the even moments (a line-strength is the zeroth moment of the LOSVD), could also be analysed by kinemetry.

We also presented a preliminary study of kinemetry of velocity fields along ellipses instead of circles. In this approach the number of terms needed to describe the field is smaller than using circles (q and c_1 versus, generally, c_1, c_3 and c_5). Also, the axial ratio, q, provides a simple way of describing the global appearance of the velocity map, which facilitates the use of illustrative terms such as *flat* or *round*. These terms are also used to describe the surface-brightness distribution (note that q can be vary significantly from case to case), and this makes a natural connection between the different moments of the distribution function.

The main assumption used when expanding along ellipses is that the velocity maps of early-type galaxies are similar to the velocity maps generated by stars moving in circular orbits in a thin disc. Although we do not suggest this as a physical interpretation for early type galaxies, it does provide an excellent low-order approximation to the observed velocity maps. Indeed, in the presented examples we found that the velocity maps of some early-type galaxies do resemble the velocity maps of discs. The presented preliminary results are encouraging and the next step is a detailed study of the kinemetry of velocity maps along ellipses for a representative sample of early-type galaxies.

Acknowledgments

We thank Eric Emsellem for providing a model axisymmetric galaxy. We thank Glenn van de Ven for many useful discussions and Richard McDermid for a critical reading of the paper.

References

Arnold R., de Zeeuw P. T., Hunter C., 1994, MNRAS, 271, 924

Bacon R., Copin Y., Monnet G., Miller B. W., Allington-Smith J. R., Bureau M., Carollo C.M., Davies R. L., et al., 2001, MNRAS, 326, 23

Begeman K. G., 1987, Ph.D. Thesis, University of Groningen

Bender R., 1988, A&A, 193, L7

Binney J., 1978, MNRAS, 183, 779

Binney J., Tremaine S., 1987, Galactic Dynamics. Princeton, NJ, Princeton University Press, 1987, 747 p.

Cappellari M., Copin Y., 2003, MNRAS, 342, 345

Davies R. L., Kuntschner H., Emsellem E., Bacon R., Bureau M., Carollo C. M., Copin Y., Miller B. W., et al., 2001, ApJ, 548, L33

de Zeeuw P. T., Bureau M., Emsellem E., Bacon R., Carollo C.M., Copin Y., Davies R. L., Kuntschner H., et al., 2002, MNRAS, 329, 513

de Zeeuw P. T., 1994, in The Formation and Evolution of Galaxies Structure, Dynamics and Formation of Spheroidal Systems, Eds. C. Muñoz-Tuñónn and F. Snchez p 231, (Cambridge: Cambridge Univ. Press)

de Zeeuw P. T., Franx M., 1989, ApJ, 343, 617

Emsellem E., Dejonghe H., Bacon R., 1999, MNRAS, 303, 495
Emsellem E., Cappellari M., Peletier R. F., McDermid R. M., Bacon R., Bureau M., Copin Y., Davies R. L., et al., 2004, MNRAS, 352, 721
Franx M., Illingworth G., de Zeeuw P. T., 1991, ApJ, 383, 112
Franx M., van Gorkom J. H., de Zeeuw P. T., 1994, ApJ, 436, 642
Gerhard O. E., 1993, MNRAS, 265, 213
Hunter C., Qian E., 1993, MNRAS, 262, 401
Jedrzejewski R. I., 1987, MNRAS, 226, 747
Lauer T. R., 1985, MNRAS, 216, 429
Schoenmakers R. H. M., Franx M., de Zeeuw P. T., 1997, MNRAS, 292, 349
Stark A. A., 1977, ApJ, 213, 368
Statler T. S., 1991, AJ, 102, 882
Statler T. S., 1994a, ApJ, 425, 458
Statler T. S., 1994b, ApJ, 425, 500
Statler T. S., Emsellem E., Peletier R. F., Bacon R., 2004, MNRAS, 353, 1
Statler T. S., Fry A. M., 1994, ApJ, 425, 481
Surma P., Bender R., 1995, A&A, 298, 405
Teuben P. J., 1991,in Warped Disks and Inclined Rings around Galaxies, eds. S. Casertano, p.D. Sackett, & F.H. Briggs, (Cambridge: Cambridge Univ. Press), p 398
van der Marel R. P., Franx M., 1993, ApJ, 407, 525
Wong T., Blitz L., Bosma A., 2004, ApJ, 605, 183